MIT Open Access Articles

Spatially Resolved Patchy Ly# Emission Within the Central Kiloparsec of a Strongly Lensed Quasar Host Galaxy at z = 2.8

Spatially Resolved Patchy Lyα Emission within the Central Kiloparsec of a Strongly Lensed Quasar Host Galaxy at $z = 2.8$

Matthew B. Bayliss[1] , Keren Sharon[2] , Ayan Acharyya[3], Michael D. Gladders[4,5], Jane R. Rigby[6] , Fuyan Bian[3,8] ,
Rongmon Bordoloi[1,9], Jessie Runnoe[2], Hakon Dahle[7] , Lisa Kewley[3] , Michael Florian[5] ,
Traci Johnson[2] , and Rachel Paterno-Mahler[2]

[1] Kavli Institute for Astrophysics and Space Research, Massachusetts Institute of Technology, 77 Massachusetts Avenue, Cambridge, MA 02139, USA
mbayliss@mit.edu
[2] Department of Astronomy, University of Michigan, 1085 S. University Avenue, Ann Arbor, MI 48109, USA
[3] RSAA, Australian National University, Cotter Road, Weston Creek, ACT 2611, Australia
[4] Kavli Institute for Cosmological Physics, University of Chicago, Chicago, IL 60637, USA
[5] Department of Astronomy and Astrophysics, University of Chicago, Chicago, IL 60637, USA
[6] Astrophysics Science Division, NASA Goddard Space Flight Center, 8800 Greenbelt Road, Greenbelt, MD 20771, USA
[7] Institute of Theoretical Astrophysics, University of Oslo, P.O. Box 1029, Blindern, NO-0315 Oslo, Norway

Abstract

We report the detection of extended Lyα emission from the host galaxy of SDSS J2222+2745, a strongly lensed quasar at $z = 2.8$. Spectroscopic follow-up clearly reveals extended Lyα in emission between two images of the central active galactic nucleus (AGN). We reconstruct the lensed quasar host galaxy in the source plane by applying a strong lens model to *HST* imaging and resolve spatial scales as small as ∼200 pc. In the source plane, we recover the host galaxy morphology to within a few hundred parsecs of the central AGN and map the extended Lyα emission to its physical origin on one side of the host galaxy at radii ∼0.5–2 kpc from the central AGN. There are clear morphological differences between the Lyα and rest-frame ultraviolet stellar continuum emission from the quasar host galaxy. Furthermore, the relative velocity profiles of quasar Lyα, host galaxy Lyα, and metal lines in outflowing gas reveal differences in the absorbing material affecting the AGN and host galaxy. These data indicate the presence of patchy local intervening gas in front of the central quasar and its host galaxy. This interpretation is consistent with the central luminous quasar being obscured across a substantial fraction of its surrounding solid angle, resulting in strong anisotropy in the exposure of the host galaxy to ionizing radiation from the AGN. This work demonstrates the power of strong-lensing-assisted studies to probe spatial scales that are currently inaccessible by other means.

Key words: galaxies: high-redshift – gravitational lensing: strong – quasars: emission lines – quasars: general

1. Introduction

All massive galaxies harbor central supermassive black holes that produce strong emission when they accrete infalling matter. This ubiquitous accretion–emission phenomenon is referred to as an AGN (Netzer 2015). Galaxies with AGNs that outshine their host galaxies ("quasars") are ubiquitous at $z \gtrsim 1$ (e.g., Pâris et al. 2017), i.e., during the epoch in which the universe formed most of its stars (Madau & Dickinson 2014). However, quasars are transient phenomena with duty cycles that are difficult to measure (Martini & Schneider 2003; Wang et al. 2006; Shen et al. 2007; Shankar et al. 2010; Schmidt et al. 2017). AGNs also acts as a source of feedback, injecting energy both radiatively and mechanically back into their immediate environments. Quasars also easily dominate the production of ionizing radiation in their local environment, even fluorescing neutral hydrogen out beyond the virial radii of the dark matter halos in which the quasars reside (e.g., Christensen et al. 2006; Smith et al. 2009; Cantalupo et al. 2014; Hennawi et al. 2015; Borisova et al. 2016; Fathivavsari et al. 2016).

Resolving the central regions of distant quasar host galaxies is challenging. Even subtracting the quasar emission with a well-understood point-spread function (PSF) in the ultraviolet

(UV) and optical can leave residual noise from the wings of the quasar emission that overwhelms the host galaxy. Recent ALMA observations at millimeter wavelengths—where the central AGN emission is less of an issue—can resolve the cold molecular gas content of distant quasar host galaxies on ∼1–2 kpc scales (Wang et al. 2013; Paraficz et al. 2017; Venemans et al. 2017). More local, low-redshift studies ($z \lesssim 0.4$) using adaptive optics and *HST* can recover host galaxy morphologies in the optical and near-infrared and find that quasar hosts can be early- or late-type galaxies (Dunlop et al. 2003; Guyon et al. 2006) and can exhibit significant star formation (e.g., Young et al. 2014). Little is known, however, about how radiation from the quasar directly affects atomic gas in their host galaxies, especially within the central kiloparsec during the era of peak quasar activity. Currently, the only way to probe these regions in the UV/optical is with high-magnification, strong-gravitational-lensing systems.

The idea of using lensed quasars to study their host galaxies is not new (e.g., Peng et al. 2006; Ross et al. 2009; Oguri et al. 2013; Rusu et al. 2014), and multiply imaged quasars with large image separations are ideal for this purpose. These are quasars lensed by groups or clusters of galaxies, with image separations (a proxy for Einstein radius) that are $\gtrsim 5''$. The large separation minimizes the confounding effects of the foreground lens light, and these systems also tend to have high magnifications over a larger area in the source plane, such

that the host galaxy is highly magnified out to physical projected radii of several kiloparsecs. Currently, there are only three large separation lensed quasars known: SDSS J1004 +4112 (Inada et al. 2003; Oguri et al. 2004; Sharon et al. 2005; Fian et al. 2016), SDSS J1029+2623 (Inada et al. 2006; Oguri et al. 2008, 2013), and SDSS J2222+2745 (Dahle et al. 2013, 2015; Sharon et al. 2017). While strong-lensing studies of these systems using *HST* can provide uniquely high spatial resolution, the technique has been relatively underutilized. This is likely attributable to two factors: the small number of suitable quasars known, and the in-depth analysis required to fully exploit the strong lensing. There is reason for optimism, however, as the number of known systems should increase in light of recent, current, and upcoming wide-field optical surveys. The increasing occurrence of strong-lensing studies of highly magnified systems bodes well. As we develop ever more expertise with lensing-assisted analyses, the tools and techniques for this work improve, and the community becomes more familiar with their potential.

In this Letter, we analyze Keck/ESI spectroscopy and *HST* imaging of the quasar, SDSS J2222+2745, and its host galaxy. The high magnification separates emission from the quasar and its host in both *HST* imaging and ground-based spectroscopy. In Section 2, we describe the data; in Section 3, we measure the relative spatial and velocity structure of Lyα in the quasar and host galaxy. We propose a physical interpretation in Section 4 and summarize our results in Section 5. We assume a flat ΛCDM cosmology with $\Omega_M = 0.3$ and $H_0 = 70 \, \mathrm{km \, s^{-1} \, Mpc^{-1}}$; in this cosmology, $1''$ corresponds to a physical scale of 7.849 kpc at the quasar redshift of $z = 2.8054$.

2. Observations and Data

2.1. SDSS J2222+2745

The lensed quasar—SDSS J2222+2745—was discovered in the Sloan Giant Arcs Survey (SGAS; Bayliss et al. 2010, 2011a, 2011b, 2014; Koester et al. 2010; Sharon et al. 2014), a systematic search for highly magnified galaxies in the Sloan Digital Sky Survey (York et al. 2000). Previous papers described the discovery and initial follow-up (Dahle et al. 2013), time delay measurements of the three brightest quasar images (Dahle et al. 2015), and detailed strong lens modeling (Sharon et al. 2017) of SDSS J2222+2745. Here, we build on previous studies of this source using the lens model from Sharon et al. (2017). SDSS J2222+2745 is at $z = 2.8$, with a luminosity that has recently varied between $L_{UV} \simeq 2$–$5 \times 10^{44} \, \mathrm{erg \, s^{-1}}$ (Dahle et al. 2015).

2.2. Keck/ESI Spectroscopy

We observed the lensed quasar and its host galaxy with the Echellette Spectrograph and Imager (ESI) on the Keck-II telescope on the nights of 2016 August 26–27 (UT dates 2016 August 27 and 2016 August 28). On the first night we targeted quasar images A and B with the $1''$ wide ESI slit at a position angle (PA) of $122°.5$ s east of north (Figure 1, dashed green), completing two 1800 s integrations. The detector was binned by two in the *x*-direction, i.e., the spatial axis along the slit.

Immediate inspection of the initial 2D spectrum revealed extended Lyα emission between the quasar A and B images (Figure 1, right panel). On the second night we observed the system again with the $6''$ wide ESI slit at a PA of $89°$ east of north, simultaneously capturing quasar images A, B, and C, as

well as the space in between these images (Figure 1, solid yellow). Our goal was to apply a "spectral imaging" mode to the entire region where the lensed quasar+host galaxy might appear. This second slit position revealed extended Lyα emission between images A and B, but nothing between images B and C (Figure 1, right panel).

We reduced the ESI spectra using a combination of IRAF tasks and the XIDL ESI pipeline developed by J. X. Prochaska[10] to subtract the bias level, apply flat-fields, and derive a wavelength map for the data. We used custom IDL routines to subtract a model of the sky flux as a function of wavelength and to extract one-dimensional spectra from several manually defined apertures for spatially distinct emission regions with the lensed quasar+host galaxy system. All observations were through light cirrus, so we recover only a relative throughput calibration as a function of wavelength using observations of two standard stars, BD +33 2642 and GD50, from the CALSPEC[11] Calibration Database.

The final $1''$ slit 1D spectra have an FWHM spectral resolution, measured from sky lines, of $R = \lambda/\Delta\lambda \simeq 5000$ ($\Delta v \simeq 60 \, \mathrm{km \, s^{-1}}$). The seeing was $\sim0''.8$, smaller than the slit width, and as a result, the spectra of the point source quasar images have slightly better spectral resolution ($R \simeq 5500$) measured for the narrowest spectral lines in the data. Unless otherwise indicated, we use spectra extracted from the $1''$ slit throughout this analysis due to the significantly lower sky background relative to the $6''$ slit data.

2.3. HST Imaging

We use *HST* imaging data from Cycle 21 program GO-13337 (PI: Sharon), described in detail in Sharon et al. (2017). Briefly, these data include *WFC3/IR* imaging in F110W and F160W, and *ACS* imaging in F435W, F606W, and F814W. These bands were selected to provide a wide lever-arm in wavelength to optimally constrain the spectral energy distributions of sources. The redder filters all sample host galaxy stellar continuum emission at $z = 2.8$, while on the blue side F435W samples a combination of far-UV stellar continuum, Lyα, and the Lyman continuum emission at the quasar redshift (Figure 2). We do not detect the host galaxy continuum spectroscopically, implying a rest-frame Lyα equivalent width, $W_0 < -20$ Å. The other filters sample the UV-through-optical continuum at $z = 2.8$: $\lambda_{\mathrm{rest, F606W}} \sim 1560$ Å, $\lambda_{\mathrm{rest, F814W}} \sim 2120$ Å, $\lambda_{\mathrm{rest, F110W}} \sim 3030$ Å, and $\lambda_{\mathrm{rest, F160W}} \sim 4040$ Å.

3. Analysis

3.1. Source Plane Reconstruction

We use the strong-lensing models and methodology described in Sharon et al. (2017) to recover lensing-corrected source plane images of the quasar host galaxy using the most highly magnified quasar image (A). We also map the ESI slit into the source plane—shown in Figure 3—which reveals the location from which the extracted host galaxy Lyα emission originates. The spatial resolution in the source plane is described by an effective lensing PSF. This lensing PSF is elliptical and varies spatially in the source plane, with FWHM

---

[10] http://www2.keck.hawaii.edu/inst/esi/ESIRedux/
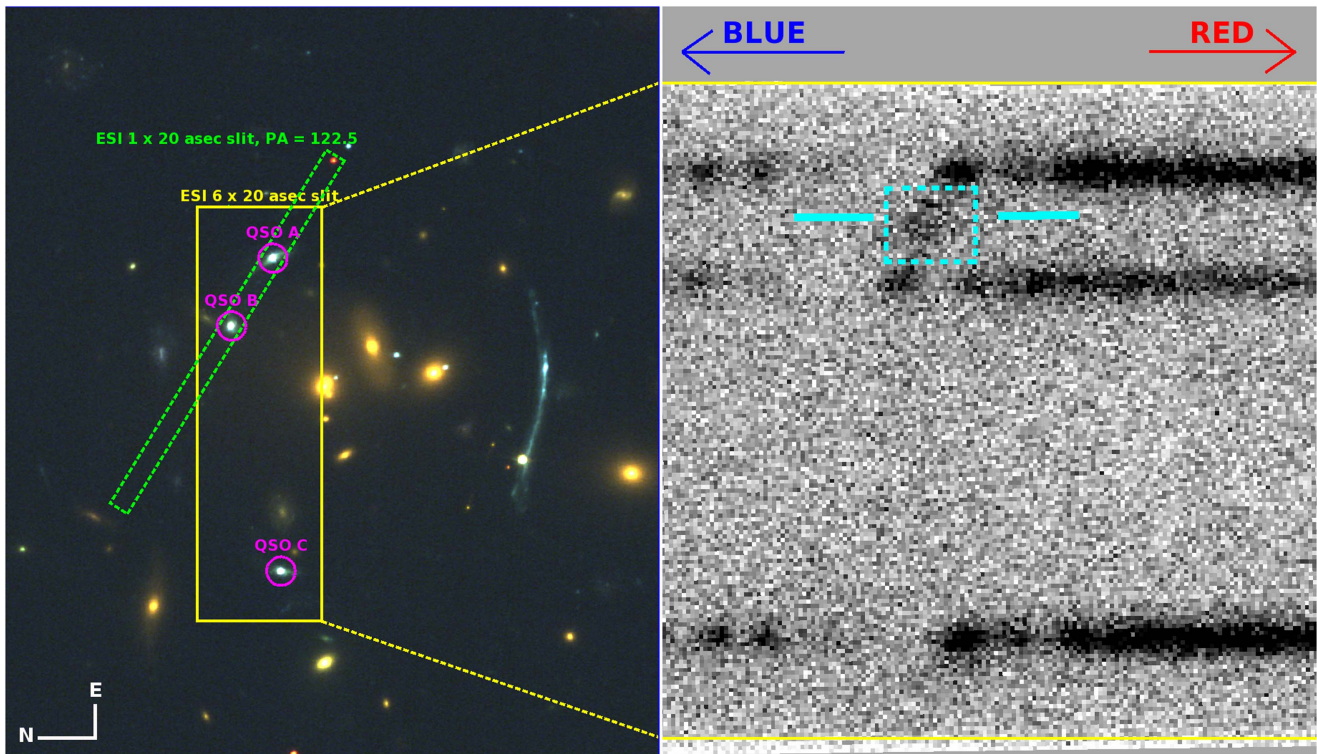[11] http://www.stsci.edu/hst/observatory/crds/calspec.html

Figure 1. Left: SDSS J2222+2745 as imaged by *HST* in bands F435W (blue), F606W (green), and F814W (red). The positions of images A, B, and C of the lensed quasar (QSO) are labeled using the conventions established in Dahle et al. (2013). The positions of both ESI observations using the $1'' \times 20''$ (green dashed; PA = 122°.5 E of N) and the $6'' \times 20''$ (solid yellow; PA $\sim 90°$ E of N) slits are also shown. Right: 2D ESI spectrum from the $6'' \times 20''$ ESI slit, zoomed in on the region containing Lyα at the quasar+host galaxy redshift ($\lambda \sim 4600$ Å); the quasar exhibits a classic asymmetric Lyα emission profile with strong emission on the red side and absorption on the blue side. Shown in 2D, the wavelength solution as a function of vertical position along the slit is no constant and depends on the horizontal position of different sources within the slit. The host galaxy Lyα emission is indicated in cyan.

values of $\sim 200 \times 500$ pc in F435W at the location of the central AGN (Figure 4).

3.2. Subtraction of the Quasar Light

We subtract the light from the quasar in the *HST* images using an isolated star $\sim 20''$ away from the quasar. We scale the peak emission of the star to that of the quasar, subtract the result from the lensed quasar images, and use the resulting quasar-subtracted image plane data to generate images of the quasar-subtracted host galaxy in the source plane. We make no attempt to recover spatial information about the host galaxy where the quasar-subtraction residuals are large. In F435W, this is an elliptical region with major and minor axes of 650 and 275 pc, respectively. The top three panels of Figure 4 show the host galaxy in the source plane in three *HST* bands that sample Lyα and the rest-frame UV, in the rest frame.

3.3. Systemic Redshift

We measure the systemic redshift using rest-frame UV features; specifically, we take a weighted average of the redshifts of O III] $\lambda 1666$ Å and C III] $\lambda\lambda 1907$, 1909 Å as measured from Gaussian fits to the line profiles. We measure a systemic redshift of $z = 2.8054 \pm 0.0004$, consistent with our previous measurement from $R \sim 1000$ spectra (Sharon et al. 2017). Recent studies show that many quasar emission lines have velocities that are biased relative to systemic as measured from stellar features (Shen et al. 2016), suggesting that our systemic redshift estimate uncertainty is dominated by systematics on the order of $\delta z \simeq 0.002$. Based on the velocities

of other features discussed below, it seems likely that the true systemic redshift of SDSS J2222+2745 is higher than our measurement by ~ 50–100 km s^{-1}.

3.4. Absorbing Outflows

The ESI spectra reveal absorption systems as traced by ionized metal-enriched gas. These systems have peculiar velocities, $v_{\rm pec}$, that are blueshifted relative to systemic, consistent with absorbing, outflowing material. Specifically, we identify a low-ionization system—likely associated with a large-scale galactic outflow—at $v_{\rm pec} = -170 \pm 10$ km s^{-1} from weak Si II $\lambda 1294$ and Fe II $\lambda 1608$ absorption. We also identify a system at $v_{\rm pec} = -240 \pm 10$ km s^{-1} that exhibits strong absorption by high-ionization lines, including N V $\lambda\lambda 1238$, 1242, C IV $\lambda\lambda 1548$, 1550, Si IV $\lambda\lambda 1393$, 1402, and He II $\lambda 1640$. A second, much weaker system at $v_{\rm pec} = -540 \pm 10$ km s^{-1} also appears in N V, C IV, and Si IV. The presence of high-ionization metals and larger outflow velocities suggest that these two system are associated with gas that is more local to the central AGN than the lower-ionization system at $v_{\rm pec} = -170$ km s^{-1}. We show the velocity profiles of Lyα and metal lines in Figure 5.

3.5. Lyα Emission

Figure 3 shows that our spectroscopic slit samples a region that extends radially away from the central AGN by ~ 0.5–2 kpc where the host galaxy has relatively low surface brightness in F435W. The larger collecting area and higher spectral resolution results in the ESI spectrum being much
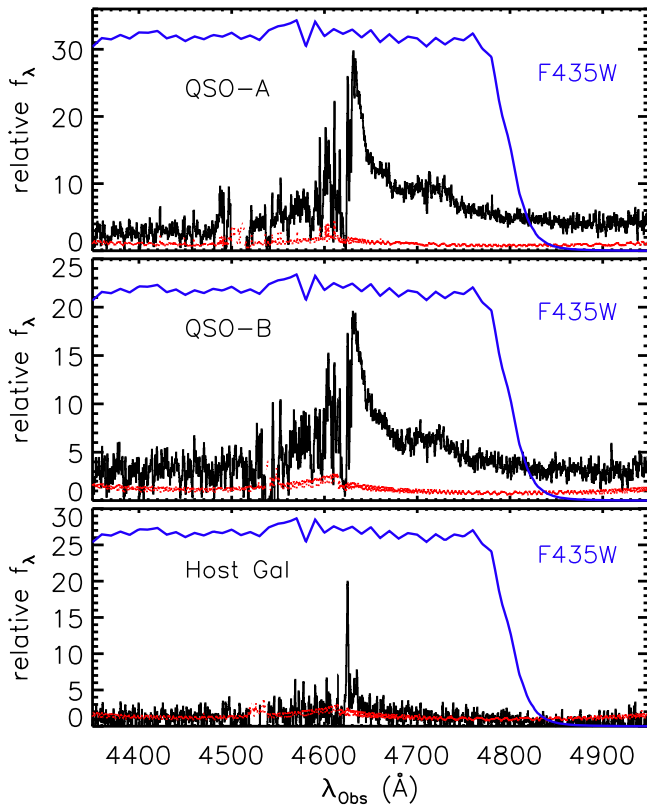
Figure 2. ESI flux (black) with error array (red) of the quasar images A and B and the host galaxy emission between $\Delta\lambda = 4350–4950$ Å, which includes Lyα ($W_0 > 20$ Å) plus rest-frame UV continuum. The host galaxy spectrum is extracted from the extended emission between the spectral traces of quasar images A and B, as indicated in Figure 1. The transmission curve of the F435W filter is overplotted in blue.

more sensitive to the Lyα emission line than the F435W imaging, with respective Lyα line surface brightness depths of $\sim 2 \times 10^{-19}$ erg s^{-1} cm^{-1} arcsec^{-2} (ESI) versus $\sim 5 \times 10^{-18}$ erg s^{-1} cm^{-1} arcsec^{-2} (F435W). The spectroscopic detection confirms relatively low-level Lyα emission across the entire host galaxy, while the F435W image reveals a strong asymmetry in the host galaxy Lyα emission (Figure 4, top left panel).

The strongest host galaxy Lyα emission in the ESI spectrum is ~ 200 km s^{-1} wide with a velocity centroid that coincides with a peak in quasar emission at $v_{pec} = -80 \pm 10$ km s^{-1}, though the host galaxy emission extends to bluer velocities than the quasar (Figure 5). The quasar emission is broad, peaking at velocities of $\sim 200–1200$ km s^{-1}, where there is only extremely weak host galaxy emission. This weak host galaxy Lyα emission has a choppy velocity structure that is unlike the redshifted Lyα emission profiles seen in starburst galaxies (e.g., Tapken et al. 2007; U et al. 2015). We verify that this weak emission does indeed originate from the host galaxy by experimenting with several extraction regions for host galaxy emission that are increasingly well separated from the A and B quasar image traces along the slit, i.e., shrinking the cyan region in Figure 3. The extended emission at $100 \lesssim v_{pec} \lesssim 500$ km s^{-1} is present independent of how conservatively we define the extraction.
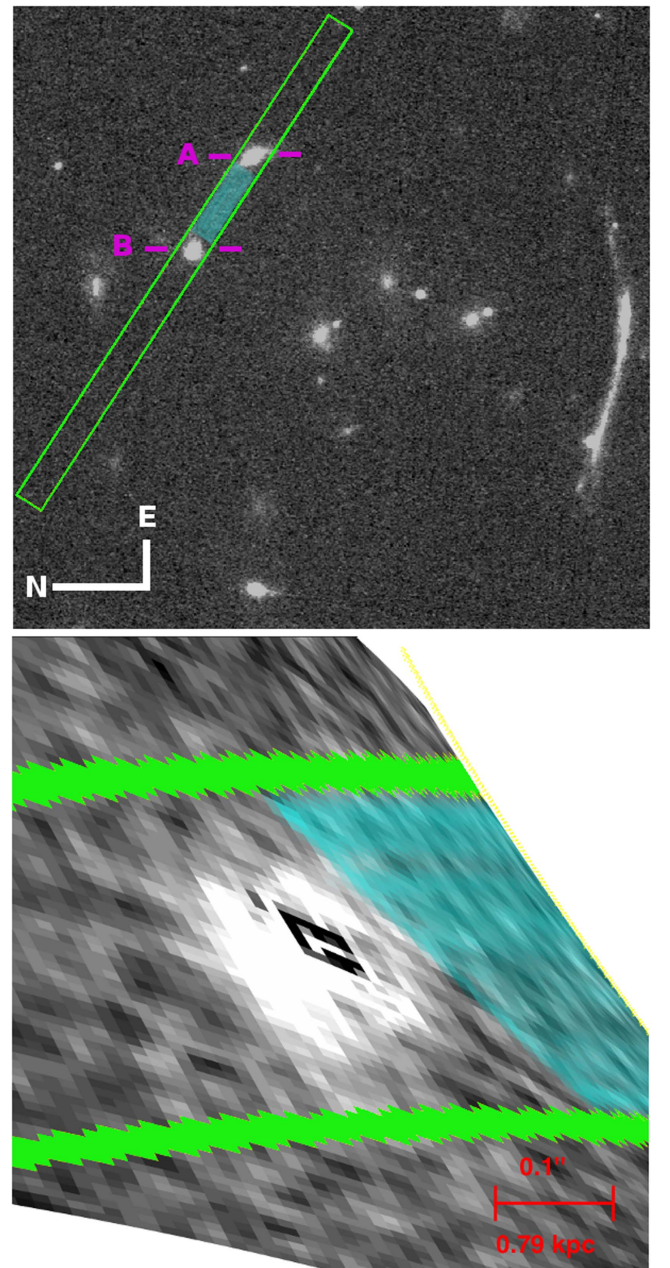

Figure 3. Top: F435W image with the $1''$ ESI slit indicated in yellow, and the region used to extract the host galaxy Lyα marked in cyan (between the traces of lensed quasar images A and B). Bottom: F435W source plane image of the quasar host galaxy, minus the quasar emission, with the $1''$ ESI slit and host galaxy Lyα extraction regions from the top panel mapped into the source plane. Due to the lensing configuration, the ESI slit samples the fainter side of the host galaxy in F435W.

4. Physical Interpretation and Discussion

The variable F435W-to-F606W flux ratio across the host galaxy implies that Lyα emission is either differently absorbed or emitted along different lines of sight toward the SDSS J2222 +2745 host galaxy. F606W and F814W sample the rest-UV stellar continuum, i.e., light associated with massive blue stars. The rest-UV color of the stellar emission is similar across the host galaxy (Figure 4, bottom rightmost panel), implying that the properties of the massive stars are similar. This implies that the
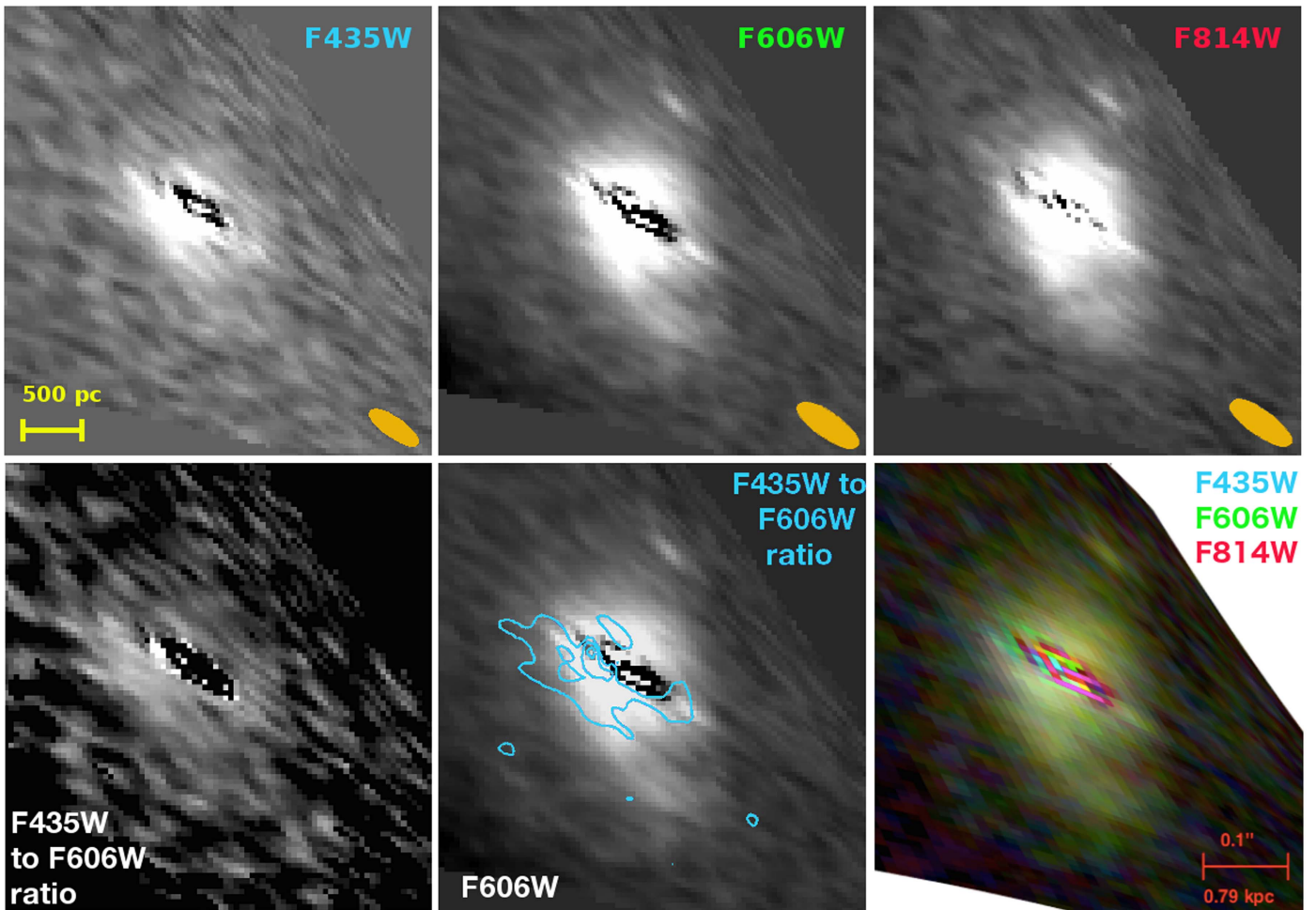
Figure 4. Top three panels: the reconstructed source plane images of the quasar host galaxy after subtracting off the AGN flux in F435W, F606W, and F814W. Orange ellipses indicate the lensing PSF at the position of the central AGN. The high magnification confines the residuals from the quasar subtraction to the central $\lesssim$200–500 pc in the bluest bands. The bottom three panels show, from right to left, the ratio of the F435W-to-F606W flux, the F606W image with the contours of the F435W-to-F606W ratio overlaid in cyan, and an RGB color image of the host galaxy made from F814W (red), F606W (green), and F435W (blue), reproduced from Sharon et al. (2017). There is a strong asymmetry to the ratio of F435W, which samples Lyα, to host galaxy stellar light as traced by F606W, and the color of the extended stellar emission is uniform across the entire host galaxy.

F606W stellar flux should map consistently to an ionizing photon flux, which would imply a relatively constant F435W/F606W ratio for Lyα emission that is powered by massive stars alone.

The F435W/F606W emission ratio in the bottom left panel of Figure 4 shows that the spatial distribution of host galaxy Lyα emission is clearly offset relative to the stellar continuum emission. This strong asymmetry in F435W/F606W and its offset relative to the stellar continuum (F606W) argue for spatial variations in one or both of: (1) the Lyα emitting gas, possibly from anisotropic illuminating ionizing radiation by the central AGN, and (2) the covering factor of intervening neutral hydrogen available to absorb Lyα. It is possible for these two effects to be related, as asymmetric escaping AGN emission could efficiently photoionize hydrogen along some sightlines into the surrounding host galaxy, while leaving significant neutral hydrogen along others. Escaping Lyα emission centered at $v_{pec} = -80$ km s^{-1} appears in both the quasar and host galaxy spectra, consistent with an approximately isotropic bubble of ionized hydrogen at a velocity near systemic. The relative velocity structures of Lyα and the outflows traced by metal absorption, shown in Figure 5, reveal that the strongest outflow system ($v_{pec} = -240$ km s^{-1}, cyan in Figure 5) is coincident with damped Lyα absorption in the quasar

spectrum, while the host galaxy Lyα emission is nonzero at the same velocity. This clear spatial decoupling of windows of Lyα escape is further evidence of differential absorption in front of the AGN versus the host galaxy.

Analysis of hundreds of luminous quasars indicates that they are typically obscured over approximately $\sim$60% of their surrounding solid angle (Polletta et al. 2008). That kind of obscuration is fully consistent with the observed asymmetry in Lyα inferred from the F435W-to-F606W ratio in SDSS J2222 +2745. It also makes sense in light of the weak host galaxy Lyα emission at $v_{pec} \sim 100$–500 km s^{-1}. This emission must result either from AGN light being scattered off of dust and gas before escaping, or from spatially extended Lyα emission from the host galaxy that is partially covered by scattering/absorbing material. Both scenarios imply the presence of more intervening gas and dust in front of the extended host galaxy than the AGN, in agreement with the physical picture outlined above in which a substantial fraction of the solid angle around the AGN is obscured.

In this interpretation, the quasar can photoionize gas along some lines of sight out of its host galaxy, but is obscured along others. The source of the obscuring material should be some combination of a dusty torus or gas and dust on large scales
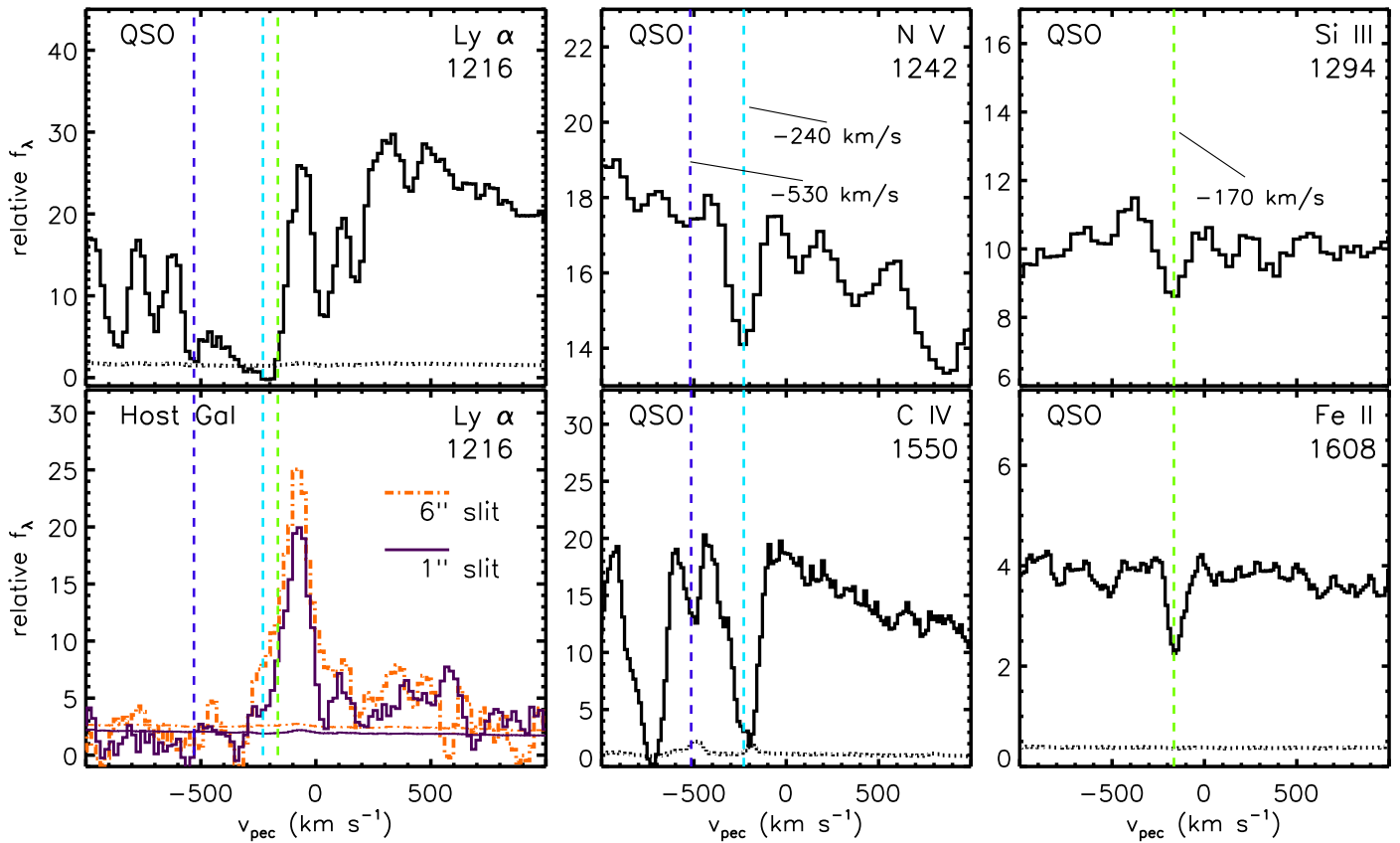
Figure 5. Velocity profiles of Lyα and metal lines present in the spectrum of lensed quasar SDSS J2222+2745 with vertical dashed lines indicating outflow velocities traced by metal lines at -530 km s^{-1} (purple), -240 km s^{-1} (cyan), and -170 (green) km s^{-1}. The leftmost two panels show the Lyα line for the quasar (top) and host galaxy (bottom), including the host galaxy spectrum extracted from the 1″ (black solid) and 6″ slits (orange dotted–dashed). The other panels show the velocity profiles of four metal lines that appear in the quasar spectra. The blue side of the host galaxy Lyα emission profile extends to velocities where the quasar Lyα is strongly absorbed, while the red side exhibits weak, choppy emission, likely resulting from either scattered AGN Lyα, or partially absorbed host galaxy emission.

(DiPompeo et al. 2016). The morphology that we observe here within the central few kiloparsecs is similar to previously observed asymmetry on approximately hundreds of kiloparsec scales in Lyα halos around distant quasars (Cantalupo et al. 2014; Hennawi et al. 2015; Borisova et al. 2016), which is also consistent with central AGNs anisotropically illuminating their surrounding environments with ionizing photons.

5. Summary

Strong gravitational lensing of SDSS J2222+2745 enables a source reconstruction of the rest-frame UV emission in the host galaxy core of this distant quasar. The ESI spectroscopy and *HST* imaging combine to reveal direct evidence of patchy structure in the Lyα emission from the host galaxy of a $z = 2.8$ quasar. We attribute this structure to anisotropic ionization and/or illumination of gas. SDSS J2222+2745 is an ideal candidate for additional follow-up to study the properties of a quasar host galaxy on sub-kiloparsec scales. Future integral field unit spectroscopy with *James Webb Space Telescope* and narrowband *HST* imaging of this and other similar systems would enable detailed emission line studies of the relative spatial and velocity structure of gas in quasar host galaxies.

ORCID iDs

Matthew B. Bayliss ◉ https://orcid.org/0000-0003-1074-4807
Keren Sharon ◉ https://orcid.org/0000-0002-7559-0864
Jane R. Rigby ◉ https://orcid.org/0000-0002-7627-6551
Fuyan Bian ◉ https://orcid.org/0000-0002-1620-0897

Bayliss et al.

Hakon Dahle ⓘ https://orcid.org/0000-0003-2200-5606
Lisa Kewley ⓘ https://orcid.org/0000-0001-8152-3943
Michael Florian ⓘ https://orcid.org/0000-0001-5097-6755
Traci Johnson ⓘ https://orcid.org/0000-0002-8829-5303

References

Bayliss, M. B., Gladders, M. D., Oguri, M., et al. 2011a, ApJL, 727, L26+
Bayliss, M. B., Hennawi, J. F., Gladders, M. D., et al. 2011b, ApJS, 193, 8
Bayliss, M. B., Rigby, J. R., Sharon, K., et al. 2014, ApJ, 790, 144
Bayliss, M. B., Wuyts, E., Sharon, K., et al. 2010, ApJ, 720, 1559
Borisova, E., Cantalupo, S., Lilly, S. J., et al. 2016, ApJ, 831, 39
Cantalupo, S., Arrigoni-Battaia, F., Prochaska, J. X., Hennawi, J. F., &
    Madau, P. 2014, Natur, 506, 63
Christensen, L., Jahnke, K., Wisotzki, L., & Sánchez, S. F. 2006, A&A,
    459, 717
Dahle, H., Gladders, M. D., Sharon, K., et al. 2013, ApJ, 773, 146
Dahle, H., Gladders, M. D., Sharon, K., Bayliss, M. B., & Rigby, J. R. 2015,
    ApJ, 813, 67
DiPompeo, M. A., Runnoe, J. C., Hickox, R. C., Myers, A. D., & Geach, J. E.
    2016, MNRAS, 460, 175
Dunlop, J. S., McLure, R. J., Kukula, M. J., et al. 2003, MNRAS, 340, 1095
Fathivavsari, H., Petitjean, P., Noterdaeme, P., et al. 2016, MNRAS, 461, 1816
Fian, C., Mediavilla, E., Hanslmeier, A., et al. 2016, ApJ, 830, 149
Guyon, O., Sanders, D. B., & Stockton, A. 2006, ApJS, 166, 89
Hennawi, J. F., Prochaska, J. X., Cantalupo, S., & Arrigoni-Battaia, F. 2015,
    Sci, 348, 779
Inada, N., Oguri, M., Morokuma, T., et al. 2006, ApJL, 653, L97
Inada, N., Oguri, M., Pindor, B., et al. 2003, Natur, 426, 810

Koester, B. P., Gladders, M. D., Hennawi, J. F., et al. 2010, ApJL, 723, L73
Madau, P., & Dickinson, M. 2014, ARA&A, 52, 415
Martini, P., & Schneider, D. P. 2003, ApJL, 597, L109
Netzer, H. 2015, ARA&A, 53, 365
Oguri, M., Inada, N., Keeton, C. R., et al. 2004, ApJ, 605, 78
Oguri, M., Ofek, E. O., Inada, N., et al. 2008, ApJL, 676, L1
Oguri, M., Schrabback, T., Jullo, E., et al. 2013, MNRAS, 429, 482
Paraficz, D., Rybak, M., McKean, J. P., et al. 2017, arXiv:1705.09931
Pâris, I., Petitjean, P., Ross, N. P., et al. 2017, A&A, 597, A79
Peng, C. Y., Impey, C. D., Rix, H.-W., et al. 2006, ApJ, 649, 616
Polletta, M., Weedman, D., Hönig, S., et al. 2008, ApJ, 675, 960
Ross, N. R., Assef, R. J., Kochanek, C. S., Falco, E., & Poindexter, S. D. 2009,
    ApJ, 702, 472
Rusu, C. E., Oguri, M., Minowa, Y., et al. 2014, MNRAS, 444, 2561
Schmidt, T. M., Worseck, G., Hennawi, J. F., Prochaska, J. X., &
    Crighton, N. H. M. 2017, arXiv:1701.08769
Shankar, F., Weinberg, D. H., & Shen, Y. 2010, MNRAS, 406, 1959
Sharon, K., Bayliss, M. B., Dahle, H., et al. 2017, ApJ, 835, 5
Sharon, K., Gladders, M. D., Rigby, J. R., et al. 2014, ApJ, 795, 50
Sharon, K., Ofek, E. O., Smith, G. P., et al. 2005, ApJL, 629, L73
Shen, Y., Brandt, W. N., Richards, G. T., et al. 2016, ApJ, 831, 7
Shen, Y., Strauss, M. A., Oguri, M., et al. 2007, AJ, 133, 2222
Smith, D. J. B., Jarvis, M. J., Simpson, C., & Martínez-Sansigre, A. 2009,
    MNRAS, 393, 309
Tapken, C., Appenzeller, I., Noll, S., et al. 2007, A&A, 467, 63
U, V., Hemmati, S., Darvish, B., et al. 2015, ApJ, 815, 57
Venemans, B. P., Walter, F., Decarli, R., et al. 2017, ApJ, 837, 146
Wang, J.-M., Chen, Y.-M., & Zhang, F. 2006, ApJL, 647, L17
Wang, R., Wagg, J., Carilli, C. L., et al. 2013, ApJ, 773, 44
York, D. G., Adelman, J., Anderson, J. E., Jr., et al. 2000, AJ, 120, 1579
Young, J. E., Eracleous, M., Shemmer, O., et al. 2014, MNRAS, 438, 217